Linear Power Flow Method for Radial Distribution Systems Including Voltage Control Devices

A. R. Di Fazio, *Member, IEEE*, S. Perna, M. Russo, *Member, IEEE*, and M. De Santis, *Member, IEEE*

***Abstract*—In large distribution systems the solution of nonlinear power flow (PF) equations requires high computational burden. To reduce complexity, various approximate linear PF methods have been proposed in literature. However, existing linear PF methods require a revision to account for new smart controllable components, introduced to increase the flexibility of distribution systems. Recently, an accurate and efficient constrained Jacobian-based method has been presented which incorporates the presence of distributed energy resources. In this paper, this method is extended to consider the presence in the network of voltage control devices (VCDs). Firstly, a new model of the supplying system is proposed to consider variations in the operating conditions of the higher voltage network, and to incorporate the presence of a VCD in the substation. Then, the most common types of direct and indirect VCDs are included into the new generalized branch model of the network. Finally, a new solving algorithm is presented which accounts for the discrete variables that are present in some VCD models, avoiding the use of any iterative procedure. The validity of the proposed method is verified by performing PF analysis on the IEEE 123-bus test feeder with VCDs and photovoltaic systems. The accuracy and the computing time of the proposed approach are analyzed by comparing them with both the exact PF and the approximated *LinDistFlow* solutions, accounting for several operating conditions of the network. The presented results give evidence of the good performance of the proposed linear method, that combines computational efficiency with adequate accuracy.**

***Index Terms*—Distribution system modeling, linear methods, voltage control devices, distributed energy resources.**

I. Introduction

A. Background and Motivation

THE evolution of distribution systems toward smart grids is essential to facilitate the widespread integration of distributed energy resources (DERs), that include distributed generators (DGs) exploiting renewable energy sources, battery storage systems, new smart loads, including charging systems for electric vehicles.

One of the most significant issues in smart distribution grids is voltage regulation. In traditional distribution systems, voltage regulation was mainly achieved by changing the ratio of the substation transformers - either manually or by automatic on-load tap changers (OLTCs) - as well as by step-voltage regulators (SVRs) and capacitor banks (CBs) along the feeders. Such voltage control devices (VCDs) are effective in regulating only slow voltage variations, and their life cycle shortens with frequent operation. In addition, the large penetration of DGs makes them unable to keep voltage within the network constraints [1]. In smart distribution grids, advanced technologies and automation must be employed for more efficient and fast voltage regulation. This involves the deployment of new devices, such as distribution static compensators (D-STATCOMs), static VAR compensators (SVCs), and unified power flow controller (UPFCs). Moreover, it is crucial to exploit the potential contribution of DERs, which provide fast and cost-effective voltage support as they are already installed in the distribution grid [2]. Recently, network reconfiguration has also been employed in voltage regulation, among other possible applications [3], [4], [5], [6].

In the near future, a large number of local VCDs will be interconnected to various nodes and distributed along different branches of a smart distribution grid. Each VCD locally regulates an electrical variable (e.g., voltage amplitude, reactive power) at a desired set-point that can be assigned either locally or calculated by voltage optimization tools [1], [7], [8]. In this latter case, not only the electrical variables are preserved within their operational ranges, but also the optimal operation of the whole distribution system can be ensured by solving a voltage optimization problem (VOP) that accounts for all the VCDs and their interactions. However, methods to control and optimize the operation of distribution grids are usually complex or problematic, due to convergence issues and the need for demanding computations that must be solved in near-real time [9]. Consequently, the practical implementation of voltage control and optimization in distribution systems requires an improvement in the computability of power flow (PF) analysis and optimization.

One of the most commonly-adopted solutions by distribution systems operators (DSOs) is to replace the non-linear PF equations with approximated linear equations, aiming to reduce model complexity and computational burden [10]. However,

Manuscript received 29 July 2023; revised 29 September 2023 and 22 November 2023; accepted 27 December 2023. Date of publication 20 February 2024; date of current version 21 May 2024. Paper 2023-PSEC-0876.R2, presented at the 2022 IEEE International Conference on Environment and Electrical Engineering and 2022 IEEE Industrial and Commercial Power Systems Europe, Prague, Czech Republic, Jun. 28–Jul. 01, and approved for publication in IEEE Transactions on Industry Applications by the Power Systems Engineering Committee of the IEEE Industry Applications Society [DOI: 10.1109/EEEIC/ICPSEurope54979.2022.9854552]. This work was supported by Project ECS 0000024 Rome Technopole, - CUP H33C22000420001, NRP Mission 4 Component 2 Investment 1.5, funded by the European Union - NextGenerationEU. *(Corresponding author: A. R. Di Fazio.)*

A. R. Di Fazio, S. Perna, and M. Russo are with the Department of Electrical and Information Engineering, University of Cassino and Southern Lazio, 03043 Cassino, Italy (e-mail: a.difazio@unicas.it).

M. De Santis is with the Department of Engineering of University of Campania "Luigi Vanvitelli", 81031 Aversa, Italy.

Color versions of one or more figures in this article are available at https://doi.org/10.1109/TIA.2024.3368009.

Digital Object Identifier 10.1109/TIA.2024.3368009

© 2024 The Authors. This work is licensed under a Creative Commons Attribution-NonCommercial-NoDerivatives 4.0 License. For more information, see https://creativecommons.org/licenses/by-nc-nd/4.0/

a drawback of this approach is the inevitable introduction of errors between the solution provided by the original model and those obtained from the linear approximation. The quality of the solution will depend on the accuracy of the linearization [11]. In addition, the applicability of existing linear PF methods may be compromised, due to the limited versatility in accommodating models of the new components of the distribution system, such as DERs and VCDs, which have a great impact on PF calculation of the distribution grid [12].

A linear power flow method based on a constrained-Jacobian approach designed for radially operated distribution systems with DERs has previously been proposed by the authors [13]. This method incorporates the full π model for lines, the ZIP model for uncontrollable loads and DERs with both active power - reactive power (P-Q) and active power - voltage (P-V) control. This approach is highly efficient in terms of computational time, because it does not require iterations to find the PF solution; moreover, it is characterized by high accuracy. Unfortunately, it does not account for the presence of VCDs in the distribution grid. To the best of the authors' knowledge, there is no extension of the linear PF model to distribution network that includes both mechanically-switched and power electronics-based VCDs. An initial study addressing this issue was proposed in [14]. The purpose of this paper is to extend and improve the work in [14], thus developing a more versatile linear PF method for distribution network with DERs and VCDs. This method is designed to exhibit high accuracy and computational efficiency; additionally, it can accommodate various configurations of the network.

B. Related Literature

Methods for approximating PF equations can be classified on the basis of their associated optimization formulations into two categories, which differ in terms of accuracy and computational efficiency: the second order convex relaxation and the constraint linearization [15]. The former is generally more accurate but it is tailored to a specific optimization problem. The latter has been proposed for its computationally-efficient formulation; moreover, linearization can be applied to a variety of problems, including control strategies, state estimation, probabilistic PF, contingency analysis, and reliability assessment [9].

A key issue in linearizing PF equations is the selection of the independent variables [16]. Two types of models are commonly employed: bus injection and branch flow [11]. A comprehensive explorations of the characteristics of bus injection models is detailed in [17]. In distribution systems, branch flow models are usually preferred over bus injection models because they better leverage the radial configuration of the grids. Moreover, bus injection models may experience poor matrix conditioning when dealing with networks that contain connected components with a high R/X ratio.

The simplest linearized PF equations based on a branch flow model is the *LinDistFlow* [18], that provides a lossless representation of the distribution system. Numerous solutions have been proposed in the literature to improve the accuracy of the *LinDistFlow* without compromising its computational efficiency. Among other approaches, a modified *LinDistFlow* is introduced in [11], which reduces the approximations by including the ratio between active (or reactive) power and the nodal voltage amplitude among the variables. Similarly, [16] demonstrates the effectiveness of using the squared amplitude rather than just the amplitude to represent the bus voltages. A linear method based on a constrained-Jacobian approach is presented in [13]. By leveraging the radial nature of the distribution network and imposing boundary conditions, it calculates the sensitivity matrices of the network in closed form. These matrices establish the relationship between branch flows and bus voltages, and the active and reactive power injections/absorptions of DERs and loads. This approach enables accurate linearization of the PF equations around an operating point. In [19], a loss approximation model is introduced for both single-phase and multi-phase *LinDistFlow*. To improve the accuracy of estimating losses and voltage profiles, the approximated expressions of higher-order terms in the Taylor series expansion of PF equations are derived in [20]. Further research on *LinDistFlow* aims to incorporate uncertainties in network parameters. For this purpose, stochastic approaches can be employed with both traditional or modified linear models, as discussed in [21]. Alternatively, data-driven techniques can be introduced, especially when a large number of historical measurements are available [10].

Linear methods require the calculation of sensitivity matrices, which are often used in control and VOPs. Given this, it becomes crucial to contain errors associated with the evaluation of sensitivity coefficients, even though they are challenging to predict. Moreover, the action of the VCDs themselves can introduce additional errors in the calculation of sensitivity coefficients [22]. Consequently, a key issue is how to account for the presence of VCDs in the linearization of PF equations.

In the literature, special attention has been dedicated to the linearization of OLTCs and CBs, considering their discrete step variations. In [23], [24], an exact linearized OLTC model is incorporated into the second-order convex relaxation of the optimal power flow (OPF) problem using a binary expansion scheme. In [25], an OPF with convex relaxation is enhanced by mixed-integer programming to account for the discrete variables associated with the OLTC positions and CBs. Since OLTCs, CBs as well as SVRs are typically slow-acting devices, VOPs are often divided into two stages; in this way, integer variables are separately optimized using mixed-integer linear programming [1], [2]. Indeed, other types of VCDs are currently being introduced into distribution networks to mitigate voltage issues arising from the widespread integration of renewable generation. Incorporating the presence of these VCDs into the general-purpose linear PF model of distribution networks is still an open issue, that requires to model and include all the VCDs with their specific characteristics (e.g., step or continuous action) and control laws. In [26] a linear PF model is enriched with a VCDs model, but the investigation is confined to the shunt VCDs with droop control laws.

C. Contributions

To overcome the shortcomings of the existing linear PF methods for distribution systems characterized by low versatility and calculation accuracy, this paper proposes a linearized model

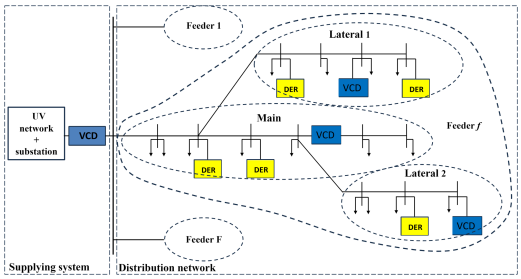

Fig. 1. Radial distribution system.

for the steady-state analysis of radial distribution grids. The proposed model incorporates various VCDs with their respective control laws as well as different types of DERs. Additionally, the discrete action of some VCDs is handled in the computational algorithm, avoiding the need of iterative procedures. This paper significantly extends our early work presented in [14]; the key contributions are outlined below.

- A more detailed modeling of the supplying system is developed to account for: i) the effects of the changes on the operating conditions of the higher voltage network to which the distribution grid is connected; and ii) the operation of the tap-changer mechanism in the substation, which can be assigned by an external signal provided by the DSO or through automatic regulation.
- The linear equations of distribution networks are extended by developing a new generalized branch model that incorporates, in addition to DERs equipped with P-Q or P-V control, VCDs located along the feeders or connected to the nodes of the grid. The VCDs are categorized into two groups. The first group acts by *directly* enforcing a controlled voltage source along the feeder (i.e., SVRs and UPFCs); the second group acts by injecting controlled powers into the node which *indirectly* alter the voltage profile (i.e., CBs, D-STATCOMs, and SVCs).
- A new algorithm capable of handling the discrete variables of some VCD models (such as OLTC and SVR with voltage regulators) is proposed; this algorithm maintains the simplicity and computational efficiency of the proposed linear method and, at the same time, avoids the use of any iterative procedures.
- In comparison to the previous work, the validity of the proposed method is tested using a more complex network, consisting of a modified 123-node network that includes OLTCs, SVRs, and photovoltaic (PV) systems; moreover, the results are compared with both the exact PF and the approximated *LinDistFlow* solutions, in terms of both accuracy and computing time, and accounting for different operating conditions of the network.

II. Distribution System Linear Modeling

Fig. 1 shows a radial distribution systems with DERs and VCDs. Models of the supplying system and the distribution network are initially presented and, then, integrated into the distribution system model. The equations are linearized and their variational expressions, defined with respect to a given initial operating condition of the distribution system, are presented in the following. The generic quantity A referred to this initial condition is represented as $(A)_0$.

A. Supplying System

The *model* of the supplying system is reported in Fig. 2(a). It includes the upper level voltage power system (HV or MV) and the substation (HV/MV or MV/LV) equipped with a VCD (i.e., OLTC in a primary substation and no-load tap changer in a secondary substation). The upstream network is represented by a no-load voltage source V_{uv} in series with the short-circuit impedance X_{cc}. The substation is divided into the branch containing the series parameters of the transformer (R_{tr} and X_{tr}) and the branch only containing the VCD. The VCD is represented by a tap changer of the transformer ratio $1 : N_{tr}$ [23]. Such a ratio can be set automatically (as in the case of primary substations) or manually (as in the case of secondary substations), depending on whether the tap changer is or is not equipped with a control system. In the first case, the tap position is determined so as to fix the voltage amplitude V_{lv} at the substation busbar or at a virtual load center by introducing a line drop compensation (LDC). The LDC settings consist of r_c and x_c (expressed in V), corresponding to the equivalent impedance between the VCD and the load center. The resulting control law is

$$V_{lv} = V_{\text{ref}} + r_c I_{lv,a} + x_c I_{lv,r} \tag{1}$$

where V_{ref} is the desired voltage reference value; $I_{lv,a}$ and $I_{lv,r}$ are, respectively, the active and reactive components of the output current of the transformer. If the VCD output (i.e., the substation busbar) is the load center, then it is $r_c = 0$ and $x_c = 0$ [27].

The *circuit equations* are derived from the Distflow equations [18]. While reference can be made to [13] for both the upstream network and the substation, the equations of the tap changer are provided below.

- Tap changer without regulator

$$\begin{aligned} P_{lv} &= P_{\bar{u}\bar{v}} \\ Q_{lv} &= Q_{\bar{u}\bar{v}} \\ V_{lv}^2 &= N_{tr}^2 V_{\bar{u}\bar{v}}^2 \quad \text{with} \quad N_{tr} = \bar{N}_{tr} \in \mathbf{N} \end{aligned} \tag{2}$$

- Tap changer with regulator (see (1))

$$\begin{aligned} P_{lv} &= P_{\bar{u}\bar{v}} \\ Q_{lv} &= Q_{\bar{u}\bar{v}} \\ V_{lv}^2 &= V_{\text{ref}} \sqrt{V_{lv}^2 + r_c P_{lv} + x_c Q_{lv}} \quad \text{with} \\ V_{lv}^2 &= N_{tr}^2 V_{\bar{u}\bar{v}}^2 \ \wedge \ N_{tr} \in \mathbf{N} \end{aligned} \tag{3}$$

where $P_{\bar{u}\bar{v}}$, $Q_{\bar{u}\bar{v}}$ and $V_{\bar{u}\bar{v}}^2$ are, respectively, the outflowing active and reactive powers, and the squared nodal voltage amplitude at the fictius node $\bar{u}\bar{v}$ of the upstream network; P_{lv}, Q_{lv} and V_{lv}^2 are the corresponding electrical quantities at the output node lv (i.e., at the substation busbar). In the absence of regulator, the transformer ratio is set to a constant value $\bar{N}_{tr}$ regardless of the load level; this value is established by solving an optimization

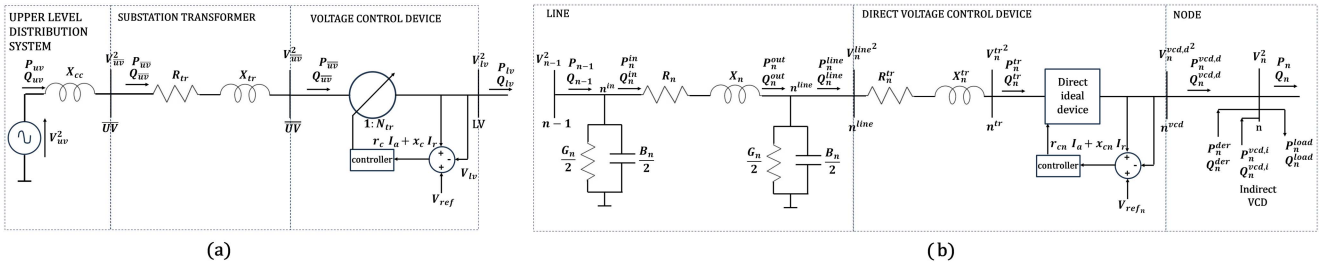

Fig. 2. Equivalent circuits: (a) Supplying system; (b) Generalized LNC.

problem or based on the DSO's experience; it is selected from a discrete set $\mathbf{N}$ by usually adjusting the tap position in regular steps (e.g., 16 raise taps and 16 lower taps). In the presence of regulator, the transformer ratio is automatically selected by the regulator that adjusts the tap position such that the load center voltage becomes the same as the reference voltage V_{ref} [28]. The discretization of the steps is discussed in Section III.

The *linear equations* of the supplying system are obtained by coupling the linear model of the upstream network, substation and VCD. The linear model of the first two components are developed in [13]. Concerning VCD, equations are derived by linearizing around an initial operating point $(\cdot)_0$ the electrical variables at the lv node in (2)–(3) with respect to the change of the same quantities at the $\bar{\bar{uv}}$ node and to the change of the VCD parameters, so that:

- Tap changer without regulator

$$\Delta \mathbf{x}_{lv} = \mathbf{J}^{tp_1} \Delta \mathbf{x}_{\bar{\bar{uv}}} + \mathbf{J}^{tp_2} \left(0,\, 0,\, \Delta N_{tr}^2\right)^{\mathrm{T}} \tag{4}$$

- Tap changer with regulator

$$\Delta \mathbf{x}_{lv} = \mathbf{J}^{tp_3} \Delta \mathbf{x}_{\bar{\bar{uv}}} + \mathbf{J}^{tp_4} \left(0,\, 0,\, \Delta V_{\text{ref}}\right)^{\mathrm{T}} \tag{5}$$

where: $\Delta \mathbf{x}_{\bar{\bar{uv}}} = (\Delta P_{\bar{\bar{uv}}}, \Delta Q_{\bar{\bar{uv}}}, \Delta V_{\bar{\bar{uv}}}^2)^T$ is the vector of the variations of the electrical variables at the $\bar{\bar{uv}}$ busbar; $\Delta \mathbf{x}_{lv} = (\Delta P_{lv}, \Delta Q_{lv}, \Delta V_{lv}^2)^T$ is the same vector at the lv busbar; and $\mathbf{J}^{tp_1}$, $\mathbf{J}^{tp_2}$, $\mathbf{J}^{tp_3}$ and $\mathbf{J}^{tp_4}$ are the Jacobian matrices, defined in Table XI in Appendix. Finally, following the approach described in [13], the linearized model of the supplying system is obtained; it linearly relates the variation of the variables of the upper voltage power system $\Delta \mathbf{x}_{uv} = (\Delta P_{uv}, \Delta Q_{uv}, \Delta V_{uv}^2)^T$ to the variations $\Delta \mathbf{x}_{lv}$ and to the variation of the VCD control parameters $\Delta \mathbf{x}^{vcd,ss}$, according to

- Tap changer without regulator

$$\Delta \mathbf{x}_{uv} = \mathbf{J}^{ss_1} \Delta \mathbf{x}_{lv} - \mathbf{J}^{ss_2} \Delta \mathbf{x}^{vcd,ss} \tag{6}$$

where

$$\mathbf{J}^{ss_1} = \mathbf{J}^{ss} (\mathbf{J}^{tp_1})^{-1},\ \mathbf{J}^{ss_2} = \mathbf{J}^{ss_1} \mathbf{J}^{tp_2},\ \Delta \mathbf{x}^{vcd,ss} = (0,\, 0,\, \Delta N_{tr}^2)^{\mathrm{T}} \tag{7}$$

- Tap changer with regulator

$$\Delta \mathbf{x}_{lv} = \mathbf{J}^{tp_3} (\mathbf{J}^{ss})^{-1} \Delta \mathbf{x}_{uv} + \mathbf{J}^{tp_4} \Delta \mathbf{x}^{vcd,ss} \tag{8}$$

where

$$\Delta \mathbf{x}^{vcd,ss} = (0,\, 0,\, \Delta V_{\text{ref}})^{\mathrm{T}} \tag{9}$$

Matrix $\mathbf{J}^{ss}$ is defined in Table XI in Appendix where $X_{eq} = X_{cc} + X_{tr}$ and $Z_{eq}^2 = R_{tr}^2 + X_{eq}^2$.

B. Distribution Network

The *model* of the distribution network is obtained by coupling the F feeder models at the lv busbar (Fig. 1). Each feeder f is modeled by combining main ($l = 0$) and laterals ($l = 1, \ldots, L_f$) that, in turns, are represented by a series of N_{f_l} generalized line-node components (LNCs). The equivalent circuit of the nth LNC is reported in Fig. 2(b). It includes the line (between node $n-1$ and n^{line}), the direct VCD (between node n^{line} and n^{vcd}), and the node n. The line is represented by the π equivalent circuit with series (R_n, X_n) and shunt (G_n, B_n) parameters. *Direct* VCDs can be SVRs or UPFCs. A SVR is an autotransformer equipped with an automatic tap-changing mechanism, that usually provides $\pm\, 10\,\%$ voltage regulation in 32 steps [27]. UPFCs are most commonly electromagnetic/power electronic devices, injecting a compensation voltage into the line through a series coupling transformer [29], [30], [31]. Both SVR and UPFC can be modeled by an equivalent impedance (similarly to a transformer with series parameters R_n^{tr} and X_n^{tr}) and by an ideal lossless device, as shown in Fig. 2(b). In the case of SVR, the device is modelled by an ideal transformer with ratio $1 : N_{tr,n}$, which is changed by steps through a tap changer [8]. Similarly to the OLTC, the tap position is set to an assigned value (typically chosen by an optimization tool of the DSO) or it varies according to the following control law

$$V_n^{vcd,d} = V_{ref,n} + r_{cn} I_a^{vcd,d} + x_{cn} I_r^{vcd,d} \tag{10}$$

where $V_{ref,n}$ is the desired reference value and r_{cn}, x_{cn} are the LDC parameters. In the case of UPFC the ideal device is modelled by a voltage generator that varies in a continuous way to impose the control law (10). Eventually, the node is modeled by a busbar with uncontrollable loads (absorbing P_n^{load} and Q_n^{load}), DERs (injecting P_n^{der} and Q_n^{der}), indirect VCDs (injecting $Q_n^{vcd,i}$, typically without active power injection (i.e., $P_n^{vcd,i} = 0$)), and laterals (deriving P_n^{lat} and Q_n^{lat}). *Indirect* VCDs can be CBs, D-STATCOMs and SVCs. Both D-STATCOMs and SVCs can provide reactive power either according to a $Q(V)$ droop control law or regulating the nodal voltage amplitude V_n to a reference value $V_{ref,n}$.

The *circuit equations* for the line of the LNC are the same as those reported in [13]. Concerning direct VCDs, they can be modeled as follows.

- *Direct VCD:* equivalent impedance

$$P_n^{tr} = P_n^{line} - R_n^{tr}\frac{P_n^{line^2} + Q_n^{line^2}}{V_n^{line^2}}$$

$$Q_n^{tr} = Q_n^{line} - X_n^{tr}\frac{P_n^{line^2} + Q_n^{line^2}}{V_n^{line^2}}$$

$$V_n^{tr^2} = V_n^{line^2} - 2(R_n^{tr}P_n^{line} + X_n^{tr}Q_n^{line}) + (R_n^{tr^2} + X_n^{tr^2})\frac{P_n^{line^2} + Q_n^{line^2}}{V_n^{line^2}} \quad (11)$$

- *Direct VCD:* ideal device

$$P_n^{vcd} = P_n^{tr}$$
$$Q_n^{vcd} = Q_n^{tr} \quad (12)$$

–SVR with assigned tap position

$$V_n^{vcd,d^2} = N_{tr,n}^2 V_n^{tr^2} \quad (13)$$

–SVR subject to the control law (10)

$$V_n^{vcd,d^2} = V_{ref,n}\sqrt{V_n^{vcd,d^2}} + r_{cn}P_n^{vcd,d} + x_{cn}Q_n^{vcd,d}$$
$$\text{with } V_n^{vcd,d^2} = N_{tr,n}^2 V_n^{tr^2} \wedge N_{tr,n} \in \mathbf{N}_{tr,n} \quad (14)$$

–UPFC subject to the control law (10)

$$V_n^{vcd,d^2} = V_{ref,n}\sqrt{V_n^{vcd,d^2}} + r_{cn}P_n^{vcd,d} + x_{cn}Q_n^{vcd,d} \quad (15)$$

Concerning the node, it is modeled by the active and reactive power balance equations. The models of uncontrollable loads (represented by the ZIP model), DERs (operating in a P-Q or a P-V control mode), and laterals are described in [13]. Concerning indirect VCDs, the CB is modeled by a discrete-varying susceptance (being $\omega C_n^{vcd,i}$ the size of a single discrete variation), whereas D-STATCOM and SVC are modeled according to their control law, so that

- *Indirect VCD:* CB

$$Q_n^{vcd,i} = \beta_n\, \omega C_n^{vcd,i}\, V_n^2 \quad \text{with } \beta_n \in \mathbf{N}_{cb,n} \quad (16)$$

- *Indirect VCD:* D-STATCOM and SVC

–with Q(V) droop control

$$Q_n^{vcd,i} = k_n^{droop}\left(V_{ref,n} - \sqrt{V_n^2}\right) \quad (17)$$

–with nodal voltage regulation

$$Q_n^{vcd,i} : V_n^2 = V_{ref,n}^2 \quad (18)$$

The discrete variations are discussed in Section III.

The *linear equations* of the LNC component in Fig. 2(b) are obtained by coupling the linear model of the line, direct VCD and node. The linear model of the line, provided in [13], is equal to

$$\Delta\mathbf{x}_n^{line} = \mathbf{J}_n^{line}\Delta\mathbf{x}_{n-1} \quad (19)$$

where: $\Delta\mathbf{x}_n^{line} = (\Delta P_n^{line}, \Delta Q_n^{line}, \Delta V_n^{line^2})^{\mathrm{T}}$ is the vector of the variations of the electrical variables at the n^{line} busbar; $\Delta\mathbf{x}_{n-1} = (\Delta P_{n-1}, \Delta Q_{n-1}, \Delta V_{n-1}^2)^{\mathrm{T}}$ is the same vector at the $n-1$ busbar; and $\mathbf{J}_n^{line}$ is the Jacobian matrix derived from the line circuit equations. Concerning direct VCD, equations are derived by linearizing (11), (12), and the appropriate equations among (13)–(15), yielding

$$\Delta\mathbf{x}_n^{vcd,d} = \mathbf{J}_n^{vcd,d_1}\Delta\mathbf{x}_n^{line} - \mathbf{J}_n^{vcd,d_2}\Delta\mathbf{x}_n^{inj,vcd} \quad (20)$$

where $\Delta\mathbf{x}_n^{vcd,d} = (\Delta P_n^{vcd,d}, \Delta Q_n^{vcd,d}, \Delta V_n^{vcd,d^2})^{\mathrm{T}}$ is the vector of the electrical variables at the n^{vcd} busbar; and $\mathbf{J}_n^{vcd,d_1}$, $\mathbf{J}_n^{vcd,d_2}$, and $\Delta\mathbf{x}_n^{inj,vcd}$ are defined below according to the type of VCD.

- *Direct VCD:* SVR with assigned tap position

$$\mathbf{J}_n^{vcd,d_1} = (\mathbf{J}_n^{id,vcd_1})^{-1}\mathbf{J}_n^{rx,vcd} \quad \mathbf{J}_n^{vcd,d_2}$$
$$= (\mathbf{J}_n^{id,vcd_1})^{-1}\mathbf{J}_n^{id,vcd_2}$$
$$\Delta\mathbf{x}_n^{inj,vcd} = (0, 0, \Delta N_{tr,n}^2)^T \quad (21)$$

- *Direct VCD:* SVR or UPFC subject to the control law (10)

$$\mathbf{J}_n^{vcd,d_1} = (\mathbf{J}_n^{id,vcd_3})^{-1}\mathbf{J}_n^{rx,vcd} \quad \mathbf{J}_n^{vcd,d_2}$$
$$= (\mathbf{J}_n^{id,vcd_3})^{-1}\mathbf{J}_n^{id,vcd_4}$$
$$\Delta\mathbf{x}_n^{inj,vcd} = (0, 0, \Delta V_{ref,n})^T \quad (22)$$

The Jacobian matrices in (21) and (22) are reported in Table XII in Appendix. The linear equations of the node for uncontrolled loads, DERs and laterals are provided in [13]. Concerning indirect VCDs, simple considerations are reported below.

- *Indirect* VCD: CB

  CBs are represented by the same linear equations as uncontrollable loads, considering only the impedance term in the ZIP model (see (16)).

- *Indirect* VCD: D-STATCOM and SVC

  –with Q(V) droop control

  It is represented by two contributions: the same linear equations as DER with PQ-control that injects only an assigned reactive power equal to $k_n^{droop}\, V_{ref,n}$ (see the first term in (17)); and the same linear equations as uncontrollable loads, considering only the current term in the ZIP model, that is equal to k_n^{droop} (see the second term in (17)).

  –with nodal voltage regulation

  It is represented by the same linear equations as DER with PV-control, being null the active power (see (18)).

Then, the generalized LNC model is obtained exactly as in [13], provided that the line model described in the previous work is replaced by the following line and direct VCD model, that is evaluated by substituting $\Delta\mathbf{x}_n^{line}$ from (19) into (20) according to

$$\Delta\mathbf{x}_n^{vcd,d} = \mathbf{J}_n^{line,vcd}\Delta\mathbf{x}_{n-1} - \mathbf{J}_n^{vcd_2}\Delta\mathbf{x}_n^{inj,vcd} \quad (23)$$

with $\mathbf{J}_n^{line,vcd} = \mathbf{J}_n^{vcd_1}\mathbf{J}_n^{line}$. Finally, by imposing the boundary conditions as in [13], the linear equations for feeders and laterals are obtained in closed form.

C. Distribution System

The *model* of the distribution system is obtained by imposing the power balance at the lv busbar between the models of the supplying system, see (6) or (8), and the distribution network.

The *linear equations* are derived according to [13], yielding

$$\boldsymbol{x}_{f,\ell,n} = (\boldsymbol{x}_{f,\ell,n})_0 + \sum_{i=1}^{F}\sum_{j=0}^{L_i}\sum_{k=1}^{N_{ij}} \mathbf{T}_{f,\ell,n}(i,j,k)\Delta\bar{\mathbf{x}}_{i,j,k}^{inj} + \boldsymbol{\lambda}_{f,\ell,n}\Delta V_{uv}^2 + \boldsymbol{\beta}_{f,\ell,n}\Delta x^{vcd,ss} \quad (24)$$

In (24) the elements of the generic 3×3 matrix $\mathbf{T}_{f,\ell,n}(i,j,k)$ are the sensitivity coefficients of the variables $\boldsymbol{x}_{f,\ell,n}$ of branch n (in the lateral ℓ of the feeder f) to the variations of injections $\Delta\bar{\mathbf{x}}_{i,j,k}^{inj}$ of branch k (in the lateral j of the feeder i) (i.e., the variations of loads, DER injections and VCD actions). The sensitivity matrices have the same formal expressions available in [13]. Concerning the others elements, $\boldsymbol{\lambda}_{f,\ell,n}$ represents the vector of sensitivity coefficients of the variables $\boldsymbol{x}_{f,\ell,n}$ with respect to the variations of the slack bus voltage ΔV_{uv}^2; whereas $\boldsymbol{\beta}_{f,\ell,n}$ represents the matrix of sensitivity coefficients of the variables $\boldsymbol{x}_{f,\ell,n}$ with respect to the action of the VCD of the supplying system $\Delta x^{vcd,ss}$, see (7) and (9). The expressions of $\boldsymbol{\lambda}_{f,\ell,n}$ and $\boldsymbol{\beta}_{f,\ell,n}$ are provided in Table XIII in Appendix and differ according to whether the VCD of the supplying system is or is not equipped with a voltage regulator.

Looking at (24), it is evident that the sets of sensitivity matrices $\mathbf{T}_{f,\ell,n}(i,j,k)$ and $\boldsymbol{\beta}_{f,\ell,n}$, and of sensitivity vectors $\boldsymbol{\lambda}_{f,\ell,n}$ are evaluated for an assigned network configuration and for a given network operating condition. Actually, different sets of matrices can be evaluated assuming some typical operating conditions (e.g., low/medium/high load level and low/rated/high voltage amplitude at the slack bus). Moreover, different sets of matrices can be evaluated for different configurations of the grid topology, if network reconfiguration is possible during operation.

The sets of sensitivity matrices are evaluated off-line. The real-time variations of the operating conditions of the distribution system $\Delta\boldsymbol{x}_{f,\ell,n} = \boldsymbol{x}_{f,\ell,n} - (\boldsymbol{x}_{f,\ell,n})_0$ caused by the variations of loads, DER injections and VCD actions $\Delta\bar{\mathbf{x}}_{i,j,k}^{inj}$ as well as by the variations of the slack bus voltage ΔV_{uv}^2 and by the action of the VCD of the supplying system $\Delta x^{vcd,ss}$ can be calculated by (24). In the real time operation of the distribution system a basic tool is the PF algorithm, which can use the model (24), as described in the next Section III.

III. Linear Power Flow Algorithm

From the linear PF equations (24) a simple algorithm can be derived. Once the various sets of coefficient matrices and vectors ($\mathbf{T}_{f,\ell,n}(i,j,k)$, $\boldsymbol{\lambda}_{f,\ell,n}$ and $\boldsymbol{\beta}_{f,\ell,n}$) are off-line calculated and stored, the on-line linear PF algorithm evaluates the effects of variations of loads, of slack bus voltage, of DER injections and of VCD actions by the straight-forward application of (24) with the appropriate sensitivity matrices.

Attention must be paid when some discrete variables are present in the VCD models, as it is the case of OLTC and SVRs. Indeed, when OLTC and SVRs are not equipped with a voltage regulator, the step discretization is simply accounted for in the tap position assignment, that is, ΔN_{tr}^2 in (7) for the OLTC and $\Delta N_{tr,n}^2$ in (21) for the SVRs.

On the contrary, when the OLTC and SVRs are subject to the control laws (1) and (10), respectively, a more complex algorithm must be implemented. In literature [22], VCD control laws with discrete steps have been accounted for by iterative algorithms. At each step of the iteration the PF equations are solved; then, the errors on the control law equations are evaluated and, on the basis of such errors, the VCD actions are corrected and used in the PF solution at the next step of the iteration. This iterative algorithm works also if the solution of the non-linear PF equations is substituted by a *LinDistFlow* algorithm.

Using the linear models presented in the previous Section II, a new non-iterative algorithm for linear PF solution is proposed hereafter. First of all, during the off-line phase, each set of sensitivity matrices is calculated twice (superscript notation is used to distinguish the two calculated sets): firstly the sets ($\mathbf{T}_{f,\ell,n}^{N}(i,j,k)$, $\boldsymbol{\lambda}_{f,\ell,n}^{N}$ and $\boldsymbol{\beta}_{f,\ell,n}^{N}$) are calculated assuming that the OLTC and SVRs are not subject to the control law but work with an assigned value of the tap position; secondly, the sets ($\mathbf{T}_{f,\ell,n}^{contr}(i,j,k)$, $\boldsymbol{\lambda}_{f,\ell,n}^{contr}$ and $\boldsymbol{\beta}_{f,\ell,n}^{contr}$) are calculated assuming that the OLTC and SVRs are subject to their control laws but their actions are continuous rather than discrete. Then, the on-line linear PF algorithm performs the following sequential steps:

1) with reference only to the supplying system and to the branches with SVRs, the electric variables in Fig. 2 are evaluated using the linear PF equations (24) using the sets $\mathbf{T}_{f,\ell,n}^{contr}(i,j,k)$, $\boldsymbol{\lambda}_{f,\ell,n}^{contr}$ and $\boldsymbol{\beta}_{f,\ell,n}^{contr}$ and considering all the injections $\Delta\bar{\mathbf{x}}_{i,j,k}^{inj}$ in the system;
2) using the results of the previous step, the transformer ratios for OLTC and SVR are evaluated, which are the ratios that satisfy the control laws in the absence of step discretization;
3) discretization is applied by choosing, for the OLTC and each SVR, the discrete tap position corresponding to the transformer ratio which is the nearest to the ratio evaluated in the previous step;
4) the linear PF equations (24) with the sets $\mathbf{T}_{f,\ell,n}^{N}(i,j,k)$, $\boldsymbol{\lambda}_{f,\ell,n}^{N}$ and $\boldsymbol{\beta}_{f,\ell,n}^{N}$ are applied to all the distribution system, assuming all the variations of injections and using the transformer ratios evaluated in the previous step.

The above procedure presents the significant advantage that it keeps the linear modeling (except for the discretization functions) and does not use any iterative procedure, thus keeping the computational burden low and avoiding any uncertainty in the computing times.

IV. Case Study

Reference is made to the IEEE 123 node test feeder described in [32], which is converted into a three-phase balanced system in view of the application of the proposed linear method (LM). Concerning the configuration of the IEEE 123 node test feeder, the normally closed switches are replaced with short-circuit connections, and the number of MV nodes is reduced from 123 to 119; the MV nodes are also renamed according to a

TABLE I
POSITION AND VOLTAGE REGULATOR SETTINGS OF OLTC AND SVRS

Type	Nodes (IEEE)	Nodes (New numer.)	V_{ref} (V)	r_c (V)	x_c (V)
OLTC	150 - 149	0 - 1	120	3.00	7.50
SVR_1	160 - 67	10 - 11	124	0.74	1.77
SVR_2	9 - 14	26 - 27	120	0.40	0.40
SVR_3	25 - 26	60 - 61	120	0.40	0.40

TABLE II
NETWORK OPERATING CONDITIONS

Case	Power level of loads (%)	Active power of DERs (kW)	Reactive power of DERs (kVAR)	Voltage regulators of VCDs
1	100	0	0	absent
2	40	0	0	absent
3	100	0	0	present
4	75	0	0	present
5	50	0	0	present
6	100	50	25	present
7	100	100	50	present
8	100	200	100	present

sequential numeration from 1 (substation MV busbar) to 119. The MV distribution network is fed by a 115/4.16 kV substation equipped with an OLTC. The HV distribution system is modeled by a no-load voltage generator $V_{uv} = 1.0$ p.u. (slack-bus) and a short-circuit power of 10^4 MVA. The HV/MV substation transformer is modelled with the series parameters $R_{tr} = 1\%$ and $X_{tr} = 8\%$, assuming a base power equal to 5 MVA. The OLTC is equipped with a regulator whose parameters are reported in Table I (i.e., connection nodes in [32], connection nodes in the new numeration, and V_{ref}, r_c, and x_c in (1)). Moreover, the case in which the OLTC operates at a specific tap position without a voltage regulator is also considered. The lines are represented by the full π model and the load absorptions are independent of the nodal voltage amplitudes; both lines and loads parameters are reported in [32]; the rated load of the feeder is equal to 3.49 MW and 1.17 MVAr. According to [32] along the distribution feeder there are 3 SVRs equipped with LDC and 4 CBs, one of 200 kVAr and three of 50 kVAr. CBs are at the IEEE nodes 83, 88, 90 and 92 and they can be entirely connected or disconnected. SVRs are equipped with regulators whose parameters are reported in Table I. Additionally, also the case where the SVRs operate at specified tap positions without the use of voltage regulators is considered. With respect to the test feeder described in [32], which refers to a passive network, 15 PV systems (PVSs) of 200 kWp each are connected to the IEEE nodes 6, 9, 16, 18, 25, 40, 51, 52, 59, 56, 57, 59, 63, 77, 105, 112, and are equipped with P-Q control.

The scope of the case study is to compare the results obtained by applying the proposed LM with those obtained using the exact PF algorithm and the classical *LinDistFlow* (LDF) algorithm. The comparison results are reported for eight cases, each representing a different operating condition of the distribution system in terms of loads, PVSs and VCDs. Specifically, Table II details the operating conditions of the distribution system in each case. The comparison is conducted in terms of the tap position of the VCDs and nodal voltage profiles, with the PF results serving as the benchmark. Additionally, the computing times of the three algorithms are also considered.

TABLE III
MAXIMUM AND AVERAGE ABSOLUTE ERRORS OF NODAL VOLTAGES FOR LM AND LDF WITH RESPECT TO PF: CASES 1, 2

	Max. abs. error (10^{-3}p.u.)		Avg. abs. error (10^{-3}p.u.)	
Cases	LM	LDF	LM	LDF
Case 1	0.27	18.7	0.18	13.8
Case 2	0.51	6.37	0.19	3.28

The presentation of the results is organized into the following three subsections by grouping the cases from Table II. The first subsection (*Cases 1–2*) analyzes the impact of assigned off-nominal tap positions of the OLTC and of the SVRs (without voltage regulators) on the load flow solutions within the passive distribution network (without PVSs). The second subsection (*Cases 3–5*) analyzes the results obtained by the three load flow algorithms when the OLTC and the SVRs are equipped with voltage regulators (see Section III), still considering the passive distribution network. Eventually, in the third subsection (*Cases 6–8*) the hypothesis of passive network is removed by adding the PVSs, while retaining the presence of voltage regulators on the OLTC and SVRs.

Algorithms have been implemented in Matlab environment and the solutions have been obtained by a laptop equipped with Intel Core i7, 2.5 GHz CPU with 16 GB of RAM.

A. OLTC and SVRs With Assigned Tap Positions

The results of the first two cases are analyzed considering the effects of different load levels and various assigned tap positions for OLTC and SVRs. The aim is to analyze the distribution system operating in extreme voltage conditions, and to compare the modelling accuracy of the LM with the one of LDF when the algorithms do not require any iteration (i.e., in absence of voltage regulators - see Section III). In detail, in *Case 1* loads are set equal to their rated values, the OLTC tap position is set to 4L, and the tap positions of the SVRs are set to 1H, so that the distribution system operates under low voltage conditions (refer to [33] for the conventional meaning of the tap positions). Conversely, in *Case 2* loads are set equal to 40% of their rated values, the OLTC tap position is set to 8H and the tap positions of the SVRs are equal to 3H, so that the distribution system operates under high voltage conditions.

Referring to the proposed LM (24), a single set of sensitivity matrices and sensitivity vectors ($\mathbf{T}_{f,\ell,n}(i,j,k)$, $\boldsymbol{\lambda}^N_{f,\ell,n}$ and $\boldsymbol{\beta}^N_{f,\ell,n}$) are evaluated and used in both the considered cases; they refers to the given configuration of the test feeder and to an initial operating condition characterized by loads absorbing the 80% of their rated powers, slack bus voltage set to 1 p.u., absence of PVSs and of VCDs.

The comparison is carried out in terms of voltage profiles, accuracy of results, and computing times. In both cases, the subsequent results are shown:

- Table III reports the maximum and average values of voltage absolute errors for LM and LDF in comparison to the exact PF solution;

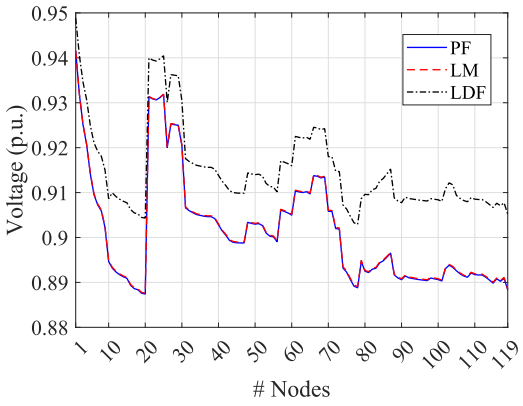

Fig. 3. Case 1: voltage profiles for PF (blue solid line), LM (red dashed line) and LDF (black dash-dotted line).

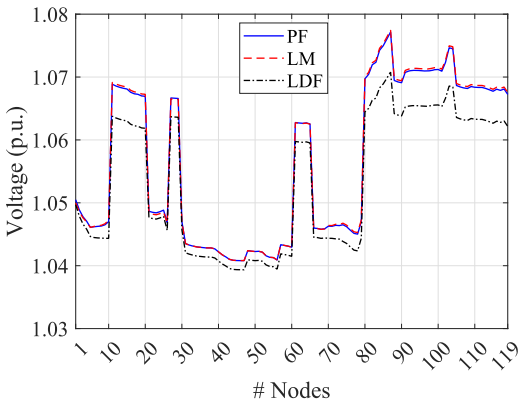

Fig. 4. Case 2: voltage profiles for PF (blue solid line), LM (red dashed line) and LDF (black dash-dotted line).

TABLE IV
AVERAGE COMPUTING TIMES (S) OF PF, LM AND LDF: CASES 1, 2

Cases	PF	LM	LDF
Case 1	0.160	0.014	0.017
Case 2	0.153	0.013	0.016

- Figs. 3 and 4 report the voltage profiles obtained by PF, LM and LDF for *Cases 1* and *2*, respectively;
- Table IV reports the average computing times of PF, LM and LDF.

Case 1 – From Fig. 3 it is apparent that, under low voltage operating conditions, the voltage profile obtained by the proposed LM is highly accurate and closely follows the profile obtained by the PF. In contrast, the LDF overestimates the voltages along the feeders. The lower accuracy of the LDF with respect to the LM is quantified in Table III by the different order of magnitude of the maximum values and of the average values of the voltage absolute errors, evaluated with respect to the nodal voltages provided by the PF. Finally, from Table IV it is apparent that the computing times of the proposed LM are similar to the ones of the LDF and of an order of magnitude smaller than the ones of the PF algorithm, which requires the iterative solution of non linear equations.

Case 2 – From Fig. 4 it is apparent that, even under high voltage operating conditions, the voltage profile obtained by the proposed LM is accurate and align the profile obtained by the PF, unlike the LDF, which underestimates the voltages along the feeders. Similarly to the previous case, Table III gives evidence of the lower accuracy of the LDF with respect to the LM, showing voltage absolute errors larger of an order of magnitude. Similar considerations to those reported for *Case 1* can be applied to the computing times in Table IV as well.

TABLE V
COMPARISON AMONG PF, LM, LDF: TAP SETTINGS OF THE VCDS IN CASES 3, 4, 5

VCD	Case 3			Case 4			Case 5		
	PF	LM	LDF	PF	LM	LDF	PF	LM	LDF
OLTC	10H	10H	8H	6H	6H	6H	3H	3H	3H
SVR_1	7H	7H	4H	6H	6H	4H	5H	5H	5H
SVR_2	3L	2L	3L	1L	1L	2L	1L	1L	1L
SVR_3	0	0	1L	0	0	1L	0	0	0

TABLE VI
MAXIMUM AND AVERAGE ABSOLUTE ERRORS OF NODAL VOLTAGES FOR LM AND LDF WITH RESPECT TO PF: CASES 3, 4, 5

	Max. abs. error (10^{-3}p.u.)		Avg. abs. error (10^{-3}p.u.)	
Cases	LM	LDF	LM	LDF
Case 3	6.03	6.02	0.76	4.47
Case 4	1.09	3.39	0.82	1.90
Case 5	0.67	2.23	0.59	1.10

B. OLTC and SVRs Equipped With Voltage Regulators

In this section, the results of three cases (*Cases 3–5*) are analyzed considering the effects of the voltage regulators in different loading conditions of the network. Equipping the OLTC and the SVRs with voltage regulators requires more complex solving algorithms as discussed in Section III.

To apply the LM algorithm, two sets of sensitivity matrices are evaluated for the adopted configuration of the test feeder and for an initial operating condition characterized by loads absorbing the 80% of their rated powers, slack bus voltage set to 1 p.u., and absence of PVSs. Concerning VCDs, both the sets of sensitivity matrices and vectors in (24), respectively ($\mathbf{T}^{N}_{f,\ell,n}(i,j,k)$, $\boldsymbol{\lambda}^{N}_{f,\ell,n}$ and $\boldsymbol{\beta}^{N}_{f,\ell,n}$) and ($\mathbf{T}^{contr}_{f,\ell,n}(i,j,k)$, $\boldsymbol{\lambda}^{contr}_{f,\ell,n}$ and $\boldsymbol{\beta}^{contr}_{f,\ell,n}$), are evaluated assuming an initial neutral tap position for the OLTC and the SVRs.

Concerning the LDF and the PF algorithms, an iterative procedure is applied to impose, by the discrete tap positions, the voltage control laws (1) and (10), respectively for the OLTC and the SVRs.

The comparison is carried out in terms of accuracy of results (i.e. tap settings of OLTC ans SVRs and nodal voltage profiles) with respect to the PF benchmark solutions, and of computing times. For all the cases, the following results are shown:

- Table V reports the VCD tap settings evaluated by PF, LM and LDF;
- Table VI reports the maximum and average values of the voltage absolute errors for LM and LDF, with respect to the exact PF solution;

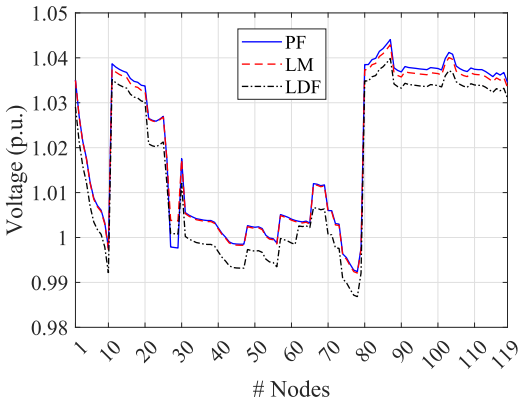

Fig. 5. Case 3: voltage profiles for PF (blue solid line), LM (red dashed line) and LDF (black dash-dotted line).

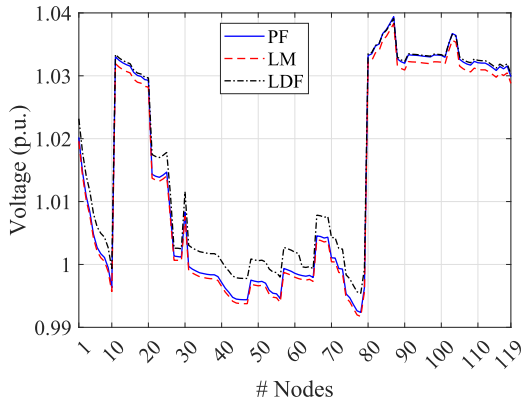

Fig. 6. Case 4: voltage profiles for PF (blue solid line), LM (red dashed line) and LDF (black dash-dotted line).

TABLE VII
AVERAGE COMPUTING TIMES (S) OF PF, LM AND LDF: CASES 3–5

Cases	PF	LM	LDF
Case 3	0.439	0.019	0.082
Case 4	0.375	0.017	0.086
Case 5	0.299	0.016	0.088

- Figs. 5–7 report the voltage profiles obtained by PF, LM and LDF for *Cases 3*, *4* and *5*, respectively;
- Table VII reports the average computing times of PF, LM and LDF.

Case 3 – The voltage profile obtained by LM is very close to the one obtained by PF (Fig. 5), except for nodes 27, 28 and 29, due to the error of LM on the tap setting of SVR_2 (2L rather than 3L), see Table V. The voltage profile obtained by LDF is more distant from the one obtained by PF than LM (Fig. 5). This is related also to the errors on tap settings of OLTC (8H rather than 10H) and SVR_1 (4H rather than 7H), see Table V. The higher accuracy of LM with respect to that of LDF is also evident by the lower average value of the voltage absolute errors ($0.76 \cdot 10^{-3}$ vs. $4.47 \cdot 10^{-3}$, see Table VI). For LM the large difference between the maximum value and the average value of the voltage absolute errors is due to the specific error on the tap setting of SVR_2; on the contrary, for LDF the maximum value and the average value of the voltage absolute errors are of the same order of magnitude. Finally, concerning the computing times of the three algorithms reported in Table VII, PF algorithm requires a computing time one order of magnitude larger than the other two algorihms, because the nonlinear PF equations must be iteratively solved. Both LM and LDF are linear methods and therefore present smaller computing times. Comparing the results in Table VII with the ones in Table IV it is evident that the computing time for LM algorithm in *Case 3* is similar to the ones of the same LM algorithm in *Cases 1* and *2*; the reason is that the algorithm also in *Case 3* does not adopt any iterative procedure, see Section III. On the contrary, the LDF algorithm performs some iterations in *Case 3* to impose the voltage control laws of the VCDs and consequently the computing time results to be approximately four times larger than the ones of the same LDF algorithm in *Cases 1* and *2* and than the one of LM algorithm in *Case 3*. For the same reason, that is the iterative procedure to account for the voltage control laws, also the computing time of PF algorithm in *Case 3* is three times larger than the ones for the same PF algorithm in *Cases 1* and *2*.

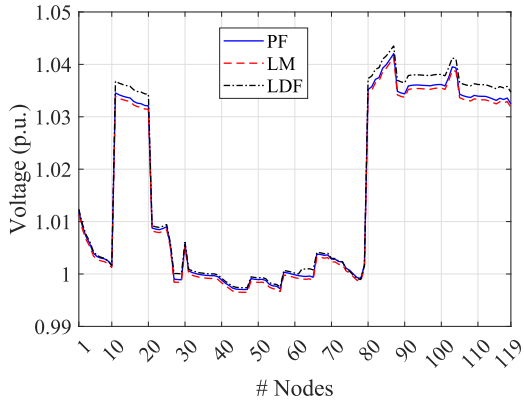

Fig. 7. Case 5: voltage profiles for PF (blue solid line), LM (red dashed line) and LDF (black dash-dotted line).

Case 4 – Concerning the voltage profiles the one obtained by LM is generally closer to that of PF than the one obtained by LDF (Fig. 6); this is confirmed by the maximum and average values of the voltage absolute errors which are lower for LM with respect to LDF (Table VI). Concerning the tap settings (Table V), the values obtained by LM are the same as those obtained by PF whereas LDF presents erroneous tap settings for all the three SVRs. Concerning the computing times of the three algorithms reported in Table VII, they are quite similar to the ones in *Case 3* and similar considerations can be made.

Case 5 – Concerning the voltage profiles the one obtained by LM is always closer to that of PF than the one obtained by LDF (Fig. 7); this is confirmed by the maximum and average values of the voltage absolute errors which are lower for LM with respect to LDF (Table VI). Concerning the tap settings, no difference is present among the three algorithms (Table V). Concerning the computing times in Table VII, they are quite similar to the ones in *Case 3* and similar considerations can be made.

TABLE VIII
COMPARISON AMONG PF, LM, LDF: TAP SETTINGS OF THE VCDS IN CASES 6, 7, 8

VCD	Case 6			Case 7			Case 8		
	PF	LM	LDF	PF	LM	LDF	PF	LM	LDF
OLTC	7H	7H	6H	4H	4H	4H	1L	2L	1L
SVR_1	7H	7H	5H	7H	6H	5H	5H	5H	6H
SVR_2	1L	2L	2L	1L	1L	1L	0	0	0
SVR_3	0	0	0	1H	0	0	1H	1H	1H

TABLE IX
MAXIMUM AND AVERAGE ABSOLUTE ERRORS OF NODAL VOLTAGES FOR LM AND LDF WITH RESPECT TO PF: CASES 6, 7, 8

	Max. abs. error (10^{-3}p.u.)		Avg. abs. error (10^{-3}p.u.)	
Cases	LM	LDF	LM	LDF
Case 6	1.09	3.24	0.71	2.31
Case 7	6.67	5.80	3.14	3.01
Case 8	1.85	5.08	1.56	2.34

TABLE X
AVERAGE COMPUTING TIMES (S) OF PF, LM AND LDF: CASES 6, 7, 8

Cases	PF	LM	LDF
Case 6	0.376	0.018	0.091
Case 7	0.385	0.017	0.090
Case 8	0.412	0.018	0.086

C. OLTC and SVRs Equipped With Voltage Regulators in Presence of PVSs

In the third group of cases (*Cases 6*, *7* and *8*), the loads are set equal to their rated values, the VCDs are equipped with voltage regulators and PVSs are connected, considering different levels of active and reactive power injections, according to Table II.

To apply the LM algorithm two sets of sensitivity matrices are evaluated for the adopted configuration of the test feeder and for an initial operating condition characterized by loads absorbing the 100% of their rated powers, slack bus voltage set to 1 p.u., and absence of PVSs. Concerning VCDs, both the sets of sensitivity matrices and vectors in (24), respectively ($\mathbf{T}^{N}_{f,\ell,n}(i,j,k)$, $\boldsymbol{\lambda}^{N}_{f,\ell,n}$ and $\boldsymbol{\beta}^{N}_{f,\ell,n}$) and ($\mathbf{T}^{contr}_{f,\ell,n}(i,j,k)$, $\boldsymbol{\lambda}^{contr}_{f,\ell,n}$ and $\boldsymbol{\beta}^{contr}_{f,\ell,n}$), are evaluated assuming an initial neutral tap position for the OLTC and the SVRs.

Concerning the LDF and the PF algorithms, an iterative procedure is applied to impose, by the discrete tap positions, the voltage control laws (1) and (10), respectively for the OLTC and the SVRs.

For all the cases, the following results are shown:

- Table VIII reports the VCD tap settings evaluated by PF, LM and LDF;
- Table IX reports the maximum and average values of voltage absolute errors for LM and LDF, with respect to the exact PF solution;
- Figs. 8–10 report the voltage profiles obtained by PF, LM and LDF for *Cases 6*, *7* and *8*, respectively;
- Table X reports the average computing times of PF, LM and LDF.

Concerning the computing times reported in Table X, they are quite similar for each algorithm and for all the *Cases 6–8* to the ones reported in Table VII in the *Cases 3–5*. Then similar considerations to the ones reported for *Case 3* can be made also for *Cases 6–8*.

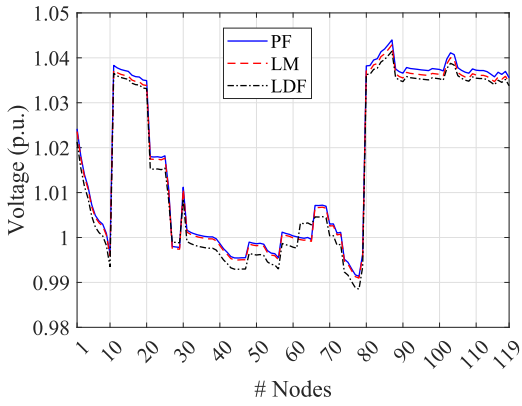

Fig. 8. Case 6: voltage profiles for PF (blue solid line), LM (red dashed line) and LDF (black dash-dotted line).

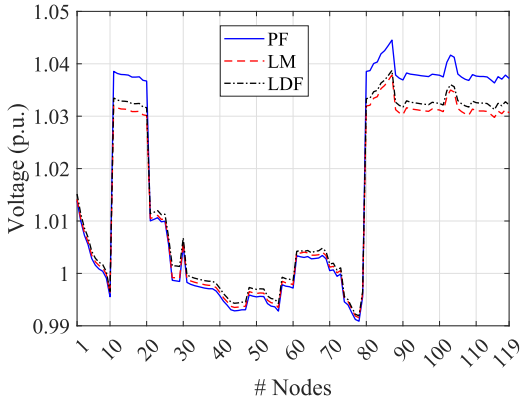

Fig. 9. Case 7: voltage profiles for PF (blue solid line), LM (red dashed line) and LDF (black dash-dotted line).

Case 6 – The voltage profile of LM is always closer to the one of PF than that of LDF (Fig. 8). The higher accuracy of LM with respect to that of LDF is confirmed by its lower values of both the average and maximum voltage absolute errors (Table IX). LM makes one error on the tap setting of SVR_2 (Table VIII), which is visible in its voltage profile at nodes 27, 28 and 29 (Fig. 8). On the contrary, LDF algorithm is mistaken the tap setting of two steps for SVR_1 and one step for OLTC and SVR_2.

Case 7 – In Fig. 9, the differences of the voltage profiles of LM and LDF with respect to that of PF are comparable. In the laterals downstream SVR_1 (where voltages are higher than 1.03 p.u. because V_{ref} for SVR_1 is 124 V on a base voltage of 120 V, see Table I), LDF performs slightly better than LM; whereas in the remaining nodes LM is closer to PF. This behavior is confirmed by the similar maximum and average values of the voltage absolute errors for LM and LDF (Table IX). Concerning the tap settings in Table VIII, LM misses one step for both SVR_1 and SVR_3 and this is the reason for the larger errors in the voltage profile downstream SVR_1. LDF algorithm is mistaken the tap settings of two steps for SVR_1 and one step for SVR_3.

Case 8 – In Fig. 10, the differences of the voltage profiles of LM and LDF with respect to that of PF are comparable. In the laterals downstream SVR_1, LM performs better than LDF

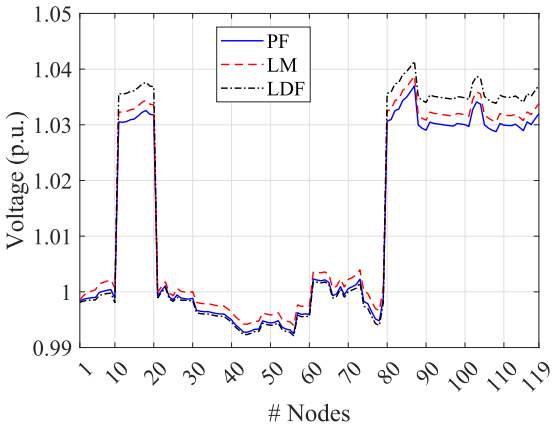

Fig. 10. Case 8: voltage profiles for PF (blue solid line), LM (red dashed line) and LDF (black dash-dotted line).

whereas in the remaining nodes LDF is slightly closer to PF. However, analyzing the results obtained for the voltage absolute errors in Table IX, the better performance of LM with respect of LDF is evident especially for the maximum value of the voltage absolute errors. Concerning the tap settings (Table VIII), LM presents only one error of one step on the tap setting of OLTC, but this mistake has limited effect on the voltage at the MV busbar (node 1, Fig. 10). The reason is related to the peculiar condition of *Case 8*, where a large amount of reactive power, generated by PVSs, flows upstream from the MV busbar to the HV system; this operating condition is very far from the initial operating condition assumed for the LM method, in which a large amount of reactive power flows downstream from HV system to the MV loads. Consequently, the LM method makes an error on the reactive power flowing upstream and on the negative voltage drop along the HV/MV transformer. This error is compensated with a different tap position yielding, however, the same voltage of about 1 p.u. on the MV busbar. Concerning LDF, it presents only one error on the tap setting of SVR_1, which causes the overestimation on the voltages downstream SVR_1, see the voltages higher than 1.03 p.u. in Fig. 10.

As a general remark, it can be concluded that the proposed LM consistently outperforms LDF in terms of accuracy when considering VCDs with assigned tap positions (first group of *Cases 1* and *2*). When the OLTC and SVRs are equipped with voltage regulators, the proposed non-iterative PF algorithm determines the tap settings of VCDs with higher accuracy than the LDF. This behaviour is observed both in the second group of cases (*Cases 3–5* where there are variations of the active and reactive powers absorbed by loads) and in the third group of cases (*Cases 6–8* where there are variations of the active and reactive powers injected by the PVSs). Additionally, it is noteworthy that the maximum absolute errors in the values of nodal voltages, obtained through the LM, are directly related to the errors in the tap settings of the VCDs located upstream of the observation nodes. This direct relationship is less evident in the case of LDF. Consequently, the results given by the LM are more reliable and more accurate, as also evidenced by the average absolute errors on the nodal voltage values which are comparable but in most cases lower than the ones of LDF. Concerning the computing times, the proposed LM algorithm presents computing times which are quite stable whichever the considered cases. With respect to the LDF algorithm, the computing times of the proposed LM are comparable in the first group of cases and significantly smaller in the second and third groups of cases. With respect to the PF algorithm, the computing times of the proposed LM are always smaller of an order of magnitude.

V. Conclusion

Power flow (PF) analysis is essential in the operation of smart distribution grids and considerable attention has been paid in literature to linear PF methods that assure an acceptable compromise between computational burden and accuracy of the solutions. However, existing linear PF methods require to be revised to account for the new smart controllable components, introduced to enhance the flexibility of distribution systems.

In this paper, a previously proposed accurate and efficient constrained Jacobian-based method, that accounts for the presence of distributed energy resources (DERs), has been extended to incorporate the models of VCDs while preserving its advantages. The method extension encompassed introducing a new model for the distribution system, specifically addressing the models of both supplying systems and branches to accommodate the presence of VCDs. Additionally, a novel algorithm was proposed for solving linear equations in load flow, taking into account the presence of discrete variables that model some specific VCDs. The validity of the proposed approach has been verified by performing PF analysis on the IEEE 123-bus test feeder including VCDs and photovoltaic systems. Results are compared with the ones obtained by both the exact non-linear PF solution and the approximated *LinDistFlow* solutions. As general conclusions, the following remarks can be stated.

- The proposed method is quite versatile because it is based on the use of sensititivy matrices and vectors that can be evaluated off-line in some given operating conditions of the distribution system, in terms of load level and network configuration; then, in the online PF analysis, the effects of DERs and of VCD actions can be evaluated by the straightforward application of the linear model.
- The novel algorithm that has been proposed adopting the proposed linear method to obtain the PF solution in presence of VCDs equipped with voltage regulators and discretized control action, such as OLTC and SVRs, is very effective; the main feature of the algorithm is that it does not need any iterative procedure and assures well defined and very limited computing times, differently from the exact non-linear PF and the *LinDistFlow* algorithms.
- The proposed linear method consistently outperforms the *LinDistFlow* in terms of accuracy, particularly when analyzing VCDs with assigned tap positions. When voltage regulators are integrated into OLTC and SVRs, the proposed non-iterative linear algorithm exhibits superior precision in determining the tap settings of VCDs compared to the *LinDistFlow*. This feature is observed in all the considered cases involving variations in active and

TABLE XI
JACOBIAN MATRICES OF THE SUPPLYING SYSTEM MODEL

$\mathbf{J}^{tp_1}$	$\mathbf{J}^{tp_2}$	$\mathbf{J}^{tp_3}$	$\mathbf{J}^{tp_4}$	$\mathbf{J}^{ss}$
$\begin{pmatrix} 1 & 0 & 0 \\ 0 & 1 & 0 \\ 0 & 0 & (N_{tr}^2)_0 \end{pmatrix}$	$\begin{pmatrix} 1 & 0 & 0 \\ 0 & 1 & 0 \\ 0 & 0 & \frac{(V_{lv}^2)_0}{(N_{tr}^2)_0} \end{pmatrix}$	$\begin{pmatrix} 1 & 0 & 0 \\ 0 & 1 & 0 \\ \frac{r_c}{1-\frac{(V_{\text{ref}})_0}{2(V_{lv})_0}} & \frac{x_c}{1-\frac{(V_{\text{ref}})_0}{2(V_{lv})_0}} & 0 \end{pmatrix}$	$\begin{pmatrix} 0 & 0 & 0 \\ 0 & 0 & 0 \\ 0 & 0 & \frac{(V_{lv})_0}{1-\frac{(V_{\text{ref}})_0}{2(V_{lv})_0}} \end{pmatrix}$	$\begin{pmatrix} 1+\frac{2R_{tr}(P_{i\bar{u}v})_0}{(V_{i\bar{u}v}^2)_0} & \frac{2R_{tr}(Q_{i\bar{u}v})_0}{(V_{i\bar{u}v}^2)_0} & -\frac{R_{tr}((P_{i\bar{u}v})_0{}^2)+(Q_{i\bar{u}v})_0{}^2)}{(V_{i\bar{u}v}^4)_0} \\ \frac{2X_{eq}(P_{i\bar{u}v})_0}{(V_{i\bar{u}v}^2)_0} & 1+\frac{2X_{eq}(Q_{i\bar{u}v})_0}{(V_{i\bar{u}v}^2)_0} & -\frac{X_{eq}((P_{i\bar{u}v})_0{}^2)+(Q_{i\bar{u}v})_0{}^2)}{(V_{i\bar{u}v}^4)_0} \\ 2R_{tr}+\frac{2Z_{eq}^2(P_{i\bar{u}v})_0}{(V_{i\bar{u}v}^2)_0} & 2X_{eq}+\frac{2Z_{eq}^2(Q_{i\bar{u}v})_0}{(V_{i\bar{u}v}^2)_0} & 1-\frac{Z_{eq}^2((P_{i\bar{u}v})_0{}^2)+(Q_{i\bar{u}v})_0{}^2)}{(V_{i\bar{u}v}^4)_0} \end{pmatrix}$

TABLE XII
JACOBIAN MATRICES OF THE DIRECT VCD MODEL

$\mathbf{J}^{id,vcd_1}$	$\mathbf{J}^{id,vcd_2}$	$\mathbf{J}^{id,vcd_3}$	$\mathbf{J}^{id,vcd_4}$	$\mathbf{J}^{rx,vcd}$
$\begin{pmatrix} 1 & 0 & 0 \\ 0 & 1 & 0 \\ 0 & 0 & (N_n^2)_0 \end{pmatrix}$	$\begin{pmatrix} 1 & 0 & 0 \\ 0 & 1 & 0 \\ 0 & 0 & \frac{(V^{vcd}{}_n^2)_0}{(N_n^2)_0} \end{pmatrix}$	$\begin{pmatrix} 1 & 0 & 0 \\ 0 & 1 & 0 \\ \frac{r_c}{1-\frac{(V_{\text{ref}})_0}{2(V_n^{vcd})_0}} & \frac{x_{c,n}}{1-\frac{(V_{\text{ref}})_0}{2(V_n^{vcd})_0}} & 0 \end{pmatrix}$	$\begin{pmatrix} 0 & 0 & 0 \\ 0 & 0 & 0 \\ 0 & 0 & \frac{(V_n^{vcd})_0}{1-\frac{(V_{\text{ref}})_0}{2(V_n^{vcd})_0}} \end{pmatrix}$	$\begin{pmatrix} 1-\frac{2R_n(P_n^{in})_0}{(V_{in}^2)_0} & \frac{-2R_n((Q_n^{in})_0}{(V_{in}^2)_0} & \frac{R_n((P_{in}^2)_0+(Q_{in}^2)_0)}{(V_{in}^4)_0} \\ \frac{-2X_n((P_n^{in})_0}{(V_{in}^2)_0} & 1-\frac{2X_n(Q_n^{in})_0}{(V_{in}^2)_0} & \frac{X_n((P_{in}^2)_0+(Q_{in}^2)_0)}{(V_{in}^4)_0} \\ -2R_n+\frac{2Z_n^2(P_n^{in})_0}{(V_{in}^4)_0} & -2X_n+\frac{2Z_n^2(Q_n^{in})_0}{(V_{in}^4)_0} & 1-\frac{Z_{eq}^2((P_{in}^2)_0+(Q_{in}^2)_0)}{(V_{in}^4)_0} \end{pmatrix}$

TABLE XIII
VECTORS AND MATRICES OF SENSITIVITY COEFFICIENTS FOR THE DISTRIBUTION SYSTEM MODEL (24)

Supplying system tap changer without voltage regulator	Supplying system tap changer with voltage regulator
$\boldsymbol{\lambda}_{f,\ell,n} = \left(\begin{bmatrix} J_{3,1}^{ss_1} & J_{3,2}^{ss_1} & 0 \end{bmatrix} \sum_{i=1}^{F} \boldsymbol{u}_{i,0,0} + J_{3,3}^{ss_1}\right)^{-1} \boldsymbol{u}_{f,\ell,n}; \quad \boldsymbol{\beta}_{f,\ell,n} = \boldsymbol{\lambda}_{f,\ell,n} \begin{bmatrix} 0 & 0 & J_{3,3}^{ss_2} \end{bmatrix}$	$\boldsymbol{\lambda}_{f,\ell,n} = \mathbf{0}; \quad \boldsymbol{\beta}_{f,\ell,n} = \left(1 - \begin{bmatrix} J_{3,1}^{tp_3} & J_{3,2}^{tp_3} & 0 \end{bmatrix} \sum_{i=1}^{F} \boldsymbol{u}_{i,0,0}\right)^{-1} \boldsymbol{u}_{f,\ell,n} \begin{bmatrix} 0 & 0 & J_{3,3}^{tp_4} \end{bmatrix}$

reactive powers absorbed by loads and injected by PV systems.

- The maximum absolute errors of the nodal voltage amplitudes obtained by the proposed linear method exhibit a direct correlation with the errors in the tap settings of the VCDs situated upstream of the observation nodes. This direct association is less evident for the *LinDistFlow*; as a result, the proposed linear method proves more reliable and accurate, as confirmed by average absolute errors in nodal voltage values that, though comparable, predominantly remain lower than those associated with the *LinDistFlow*.

Future research will investigate the extension of the proposed method to unbalanced three-phase systems.

APPENDIX

The Jacobian matrices of Section II are reported in Table XI for the supplying system and in Table XII for the direct VCD. The sensitivity vectors of (24) are reported in Table XIII; refer to [13] for the definition of $\boldsymbol{u}_{f,\ell,n}$.

REFERENCES

[1] A. R. D. Fazio, C. Risi, M. Russo, and M. D. Santis, "Coordinated optimization for zone-based voltage control in distribution grids," *IEEE Trans. Ind. Appl.*, vol. 58, no. 1, pp. 173–184, Jan./Feb. 2022.

[2] A. Savasci, A. Inaolaji, and S. Paudyal, "Two-stage volt-var optimization of distribution grids with smart inverters and legacy devices," *IEEE Trans. Ind. Appl.*, vol. 58, no. 5, pp. 5711–5723, Sep./Oct. 2022.

[3] M. R. Dorostkar-Ghamsari, M. Fotuhi-Firuzabad, M. Lehtonen, and A. Safdarian, "Value of distribution network reconfiguration in presence of renewable energy resources," *IEEE Trans. Power Syst.*, vol. 31, no. 3, pp. 1879–1888, May 2016.

[4] Y. Song, Y. Zheng, T. Liu, S. Lei, and D. J. Hill, "A new formulation of distribution network reconfiguration for reducing the voltage volatility induced by distributed generation," *IEEE Trans. Power Syst.*, vol. 35, no. 1, pp. 496–507, Jan. 2020.

[5] Y. Liu, J. Li, and L. Wu, "Coordinated optimal network reconfiguration and voltage regulator/DER control for unbalanced distribution systems," *IEEE Trans. Smart Grid*, vol. 10, no. 3, pp. 2912–2922, May 2019.

[6] A. Asrari, S. Lotfifard, and M. Ansari, "Reconfiguration of smart distribution systems with time varying loads using parallel computing," *IEEE Trans. Smart Grid*, vol. 7, no. 6, pp. 2713–2723, Nov. 2016.

[7] H. Sun et al., "Review of challenges and research opportunities for voltage control in smart grids," *IEEE Trans. Power Syst.*, vol. 34, no. 4, pp. 2790–2801, Jul. 2019.

[8] K. M. Muttaqi, A. D. T. Le, M. Negnevitsky, and G. Ledwich, "A coordinated voltage control approach for coordination of OLTC, voltage regulator, and DG to regulate voltage in a distribution feeder," *IEEE Trans. Ind. Appl.*, vol. 51, no. 2, pp. 1239–1248, Mar./Apr. 2015.

[9] J. Huang, B. Cui, X. Zhou, and A. Bernstein, "A generalized lindistflow model for power flow analysis," in *Proc. 60th IEEE Conf. Decis. Control*, 2021, pp. 3493–3500.

[10] M. Marković and H. Bri-Mathias, "Parameterized linear power flow for high fidelity voltage solutions in distribution systems," *IEEE Trans. Power Syst.*, vol. 38, no. 5, pp. 4391–4403, Sep. 2022.

[11] T. Yang, Y. Guo, L. Deng, H. Sun, and W. Wu, "A linear branch flow model for radial distribution networks and its application to reactive power optimization and network reconfiguration," *IEEE Trans. Smart Grid*, vol. 12, no. 3, pp. 2027–2036, May 2021.

[12] K. Liu, C. Wang, W. Wang, Y. Chen, and H. Wu, "Linear power flow calculation of distribution networks with distributed generation," *IEEE Access*, vol. 7, pp. 44686–44695, 2019.

[13] A. R. D. Fazio, M. Russo, S. Valeri, and M. D. Santis, "Linear method for steady-state analysis of radial distribution systems," *Int. J. Elect. Power Energy Syst.*, vol. 99, pp. 744–755, 2018.

[14] A. R. D. Fazio, S. Perna, M. Russo, and M. D. Santis, "Linear method for radial distribution systems including voltage control devices," in *Proc. IEEE Int. Conf. Environ. Elect. Eng., IEEE Ind. Commercial Power Syst. Eur.*, 2022, pp. 1–8.

[15] D. K. Molzahn and I. A. Hiskens, "A survey of relaxations and approximations of the power flow equations," *Found. Trends Elect. Energy Syst.*, vol. 4, no. 1/2, pp. 110–138, 2019, doi: 10.1561/3100000012.

[16] Z. Yang, K. Xie, J. Yu, H. Zhong, N. Zhang, and Q. Xia, "A general formulation of linear power flow models: Basic theory and error analysis," *IEEE Trans. Power Syst.*, vol. 34, no. 2, pp. 1315–1324, Mar. 2019.

[17] A. Bernstein, C. Wang, E. Dall'Anese, J.-Y. Le Boudec, and C. Zhao, "Load flow in multiphase distribution networks: Existence, uniqueness, non-singularity and linear models," *IEEE Trans. Power Syst.*, vol. 33, no. 6, pp. 5832–5843, Nov. 2018.

[18] M. Baran and F. Wu, "Network reconfiguration in distribution systems for loss reduction and load balancing," *IEEE Trans. Power Del.*, vol. 4, no. 2, pp. 1401–1407, Apr. 1989.

[19] E. Schweitzer, S. Saha, A. Scaglione, N. G. Johnson, and D. Arnold, "Lossy distflow formulation for single and multiphase radial feeders," *IEEE Trans. Power Syst.*, vol. 35, no. 3, pp. 1758–1768, May 2020.

[20] R. A. Jabr, "High-order approximate power flow solutions and circular arithmetic applications," *IEEE Trans. Power Syst.*, vol. 34, no. 6, pp. 5053–5062, Nov. 2019.

[21] N. Rashidirad, H. Dagdougui, and K. Sheshyekani, "A novel approach for improved linear power-flow formulation," *IEEE Trans. Power Del.*, vol. 37, no. 6, pp. 5224–5233, Dec. 2022.

[22] F. J. Zarco-Soto, J. L. Martínez-Ramos, and P. J. Zarco-Periñán, "A novel formulation to compute sensitivities to solve congestions and voltage problems in active distribution networks," *IEEE Access*, vol. 9, pp. 60713–60723, 2021.

[23] W. Wu, Z. Tian, and B. Zhang, "An exact linearization method for OLTC of transformer in branch flow model," *IEEE Trans. Power Syst.*, vol. 32, no. 3, pp. 2475–2476, May 2017.

[24] X. Chen, W. Wu, and B. Zhang, "Robust capacity assessment of distributed generation in unbalanced distribution networks incorporating ANM techniques," *IEEE Trans. Sustain. Energy*, vol. 9, no. 2, pp. 651–663, Apr. 2018.

[25] S. R. Shukla, S. Paudyal, and M. R. Almassalkhi, "Efficient distribution system optimal power flow with discrete control of load tap changers," *IEEE Trans. Power Syst.*, vol. 34, no. 4, pp. 2970–2979, Jul. 2019.

[26] Y. Tan, C. Liao, Y. Li, Y. Cao, M. Shahidehpour, and C. Chen, "A linear power flow model for balanced distribution network with droop-controlled dstatcom and voltage controlled DG," *Int. J. Elect. Power Energy Syst.*, vol. 117, 2020, Art. no. 105665. [Online]. Available: https://www.sciencedirect.com/science/article/pii/S0142061518328618

[27] W. Kersting, *Distribution System Modeling and Analysis*, 3rd ed. Boca Raton, FL, USA: CRC Press, Taylor and Francis Group, ch. 5–Power Flow Approximations, 2012.

[28] K.-H. Yoon, J.-W. Shin, T.-Y. Nam, J.-C. Kim, and W.-S. Moon, "Operation method of on-load tap changer on main transformer considering reverse power flow in distribution system connected with high penetration on photovoltaic system," *Energies*, vol. 15, no. 6473, pp. 1–17, 2022.

[29] M. M. Haque, M. S. Ali, P. Wolfs, and F. Blaabjerg, "A UPFC for voltage regulation in LV distribution feeders with a dc-link ripple voltage suppression technique," *IEEE Trans. Ind. Appl.*, vol. 56, no. 6, pp. 6857–6870, Nov./Dec. 2020.

[30] B. K C, A. Verma, and S. K. Chattopadhyay, "Flexible step-voltage regulator for unbalanced distribution networks," *IEEE Trans. Ind. Appl.*, vol. 58, no. 6, pp. 7002–7012, Nov./Dec. 2022.

[31] J. Yuan, S. Xu, H. Chen, C. Zou, Y. Ji, and S. Yin, "A novel multiline fast electromagnetic unified power flow controller topology for distribution network," *IEEE Trans. Ind. Appl.*, vol. 58, no. 3, pp. 3238–3249, May/Jun. 2022.

[32] IEEE PES AMPS DSAS Test Feeder Working Group "IEEE Test Feeders," 1992. Accessed: Jul. 26, 2023 [Online]. Available: https://site.ieee.org/pes-testfeeders/resources/

[33] R. Anilkumar, G. Devriese, and A.K. Srivastava, "Voltage and reactive power control to maximize the energy savings in power distribution system with wind energy," *IEEE Trans. Ind. Appl.*, vol. 54, no. 1, pp. 656–664, Jan./Feb. 2018.

Open Access provided by 'Università degli Studi di Cassino e del Lazio Meridionale' within the CRUI CARE Agreement